Biophysical Journal Volume 106 June 2014 2322–2329

Hyperglycemic and Hyperlipidemic Conditions Alter Cardiac Cell Biomechanical Properties

Jarett Michaelson, Venkatesh Hariharan, and Hayden Huang*
Department of Biomedical Engineering, Columbia University, New York, New York

ABSTRACT Currently, many diabetic cardiomyopathy (DC) studies focus on either in vitro molecular pathways or in vivo whole-heart properties such as ejection fraction. However, as DC is primarily a disease caused by changes in structural and functional properties, such studies may not precisely identify the influence of hyperglycemia or hyperlipidemia in producing specific cellular changes, such as increased myocardial stiffness or diastolic dysfunction. To address this need, we developed an in vitro approach to examine how structural and functional properties may change as a result of a diabetic environment. Particle-tracking microrheology was used to characterize the biomechanical properties of cardiac myocytes and fibroblasts under hyperglycemia or hyperlipidemic conditions. We showed that myocytes, but not fibroblasts, exhibited increased stiffness under diabetic conditions. Hyperlipidemia, but not hyperglycemia, led to increased cFos expression. Although direct application of reactive oxygen species had only limited effects that altered myocyte properties, the antioxidant N-acetylcysteine had broader effects in limiting glucose or fatty-acid alterations. Changes consistent with clinical DC alterations occur in cells cultured in elevated glucose or fatty acids. However, the individual roles of glucose, reactive oxygen species, and fatty acids are varied, suggesting multiple pathway involvement.

INTRODUCTION

Cardiovascular diseases account for ~80% of deaths associated with diabetes mellitus, primarily through coronary artery disease (1). However, a relatively new clinical entry, termed diabetic cardiomyopathy (DC), produces heart failure in diabetic patients independently of coronary artery disease or hypertension (2,3). In DC, hyperglycemia and hyperlipidemia are thought to produce structural and biochemical alterations leading to major functional changes in the myocardium, which can lead to diastolic and systolic dysfunction, and eventually to heart failure (4–6). Early-stage alterations include hypertrophy, calcium mishandling, apoptosis, excessive reactive oxygen species (ROS) production, and increased collagen production by fibroblasts (7–13). Although many of the signs of DC have been characterized, disease progression is not well understood, particularly at the early stage of the condition, thus limiting the ability of researchers to develop treatment options.

Currently, the majority of DC studies focus either on in vitro molecular pathway studies or in vivo whole-heart measurements. However, as DC is primarily a disease of changes in structural and functional properties in mechanically active tissue, these studies incompletely delineate potential biomechanical factors underlying these changes. In particular, we wish to isolate the effects of elevated glucose or fatty acids on the cardiac myocytes themselves. In vivo, this would be difficult, as systemic changes may result in, for example, alterations in release of compounds from noncardiac tissue that affect the heart. Therefore, we developed an in vitro approach for measuring key cardiac cell structural and functional properties. For example, increased myocardial stiffness, which is a major contributor to diastolic dysfunction, is currently associated with increased collagen production in the heart (14,15). However, diastolic dysfunction can occur in DC before significant collagen accumulates (16). Thus, it is possible that cellular alterations, rather than cardiac fibrosis, contribute to diastolic dysfunction.

Our hypothesis is that alterations to cellular biomechanical properties, as well as key biomechanically linked pathways (hypertrophy), occur at the cardiac cellular level in response to the diabetic conditions of hyperglycemia or hyperlipidemia. For example, increased cardiac cell stiffness could contribute to early-stage increases in myocardial stiffness before the later stages of diabetic heart failure (17). In testing this hypothesis, we isolated the effects of direct diabetic conditions from potential extracardiac influences. To assess whether cardiac-specific changes occur, and whether they are consistent with DC progression, we first deployed particle-tracking microrheology in cardiac myocytes, fibroblasts, and coculture of myocytes and fibroblasts to assess the effects of elevated glucose or PA on cellular biomechanical properties. For the coculture assay, myocytes and fibroblasts were plated in bilayers to better mimic the complex layered structure of the heart, and to more accurately assess the effects of DC conditions on cardiac cell mechanical properties. In addition, by comparing the mechanical properties of cardiac cells in a cocultured bilayer against their properties in a monolayer, we can assess whether the structural and biochemical interactions between the two types of cell have significant impact on their mechanical properties.

Submitted October 29, 2013, and accepted for publication April 28, 2014.
*Correspondence: hayden.huang@columbia.edu
Editor: Levi Gheber.

0006-3495/14/06/2322/8 $2.00
http://dx.doi.org/10.1016/j.bpj.2014.04.040

We then investigated the potential role of ROS in mediating biomechanical changes associated with diabetes. Elevation of ROS can lead to cellular damage by oxidation by interfering with nitric oxide (NO) and by modulating redox signaling pathways (18). Oxidative stress is implicated in all stages of DC, including hypertrophy, fibrosis, and contractile dysfunction (19). We also assessed the effects of the antioxidant N-acetylcysteine (NAC) toward reversing changes in cell biomechanical properties (7,20). Finally, we assessed the role of diabetic culture conditions on the hypertrophic indicator cFos, which is a key regulator of cardiac hypertrophy and may be implicated in DC progression (21,22). We found that there are significant cell-level alterations that are consistent with DC progression, but that the precise role of glucose versus fatty acids, and of ROS, in mediating these alterations, is not clear-cut.

METHODS

Cell culture

Unless otherwise specified, components were acquired from Life Technologies (Norwalk, CT).

Primary neonatal rat cardiomyocytes (CMs) were obtained from minced hearts after euthanasia via decapitation and were cultured using M199 containing 10% neonatal calf serum (NCS), penicillin/streptomycin (PS), 0.1 mM 5-bromo-2-deoxyuridine (BrdU) (Sigma, St. Louis, MO), and 0.2 mM epinephrine (Sigma) (CM plating media), and were incubated at 37°C and 1% CO_2. For all high-glucose experiments, except where specified, on the day after the isolation, the medium was replaced with M199 containing 5% NCS, PS, and BrdU, with either 5.5 mM (low glucose (LG)) or 30.5 mM D-Glucose (high glucose (HG)) (Sigma). The myocytes were then cultured for 2 days before the start of experiments. The 0.5 mM palmitic acid (PA) and BSA-only medium was made according to a previously established protocol (23). In brief, PA (Sigma) was dissolved in ethanol to a concentration of 195 mM before being diluted in LG (5.5 mM) M199 to its final concentration (0.5 mM). As a vehicle for the PA, fatty-acid-free BSA was also added to the medium at a 1:6 molar ratio of the PA (23). The medium was supplemented with 20% NCS, PS, and BrdU. Unless otherwise stated, cells used in the high-fatty-acid experiments were treated with either 0.5 mM PA or BSA-only control medium for 24 h before data were taken. The media was supplemented with 20% fetal calf serum in all cases for CMs used for the cFos western blot, as cFos levels were not detectable with 5% NCS. For NAC (Sigma) treatment, NAC was added to media at concentration of 1uM. For the hydrogen peroxide (HP) experiments, CMs were treated with HP in LG control media for 24 hr prior to imaging or cell lysis (for immunoblotting).

Cardiac fibroblasts (CFs) were obtained via the same isolation as the CMs and cultured using Dulbecco's modified Eagle's medium containing 10% fetal calf serum and PS, and were incubated at 37°C and 5% CO_2. When the CFs were ~90% confluent, they were treated with serum-free media for 2 h to render them quiescent (to ensure that all CFs were treated with HG/PA for equivalent time). Except where noted, the CFs were then treated with either HG or high fatty acid media (same as CM media, except with Dulbecco's modified Eagle's medium in place of M199 and with no serum) for 48 and 24 h, respectively, before experiments were begun. This investigation conforms to the Guide for the Care of Use of Laboratory Animals as approved by the Columbia Institute of Comparative Medicine.

Particle-tracking microrheology experimental setup for monolayer

For cardiac myocyte and cardiac fibroblast monolayers, dishes were seeded with 1 μm fluorescent probes (Life Technologies) 24 h before the start of experiments. Due to the fragile nature of the cardiac myocyte monolayer, the fluorescent probes were introduced to the cells via endocytosis. Other techniques, such as microinjection and blast injection, were found to cause too much damage to the cell or monolayer to be used for the study. Although endocytosis does introduce the possibility of active motion via vesicle formation, Jonas et al. found that neutralization of vesicles via chloriquine had no significant effect on mechanical properties in an endocytosis-based microrheology study (24). To arrest spontaneous contraction, myocytes were treated with 100 mM KCl (Sigma) in Hank's buffered salt solution (HBSS) without calcium or magnesium for 1 h before the start of experiments. Both cardiac myocytes and fibroblasts were maintained at 37°C during imaging. Bead trajectories were acquired for ~1 min at 16 Hz using a 100× (1.3 NA) objective.

Particle-tracking microrheology analysis for monolayers

Beads were tracked and their trajectory analyzed as previously described (25,26). Briefly, trajectories were extracted using a custom multiple-particle-tracking MATLAB (The Mathworks, Natick, MA) program (25,26). The change in position of particles was tracked over all frames, correcting for whole-field shifting (motion of the stage or dish). The mean-squared displacement (MSD) was obtained by averaging over the squared displacements of all particles at various time lags:

$$\left\langle \Delta r^2(\tau) \right\rangle = \left\langle (r(t+\tau) - r(t))^2 \right\rangle_t,$$

where $r(t)$ describes the particle's two-dimensional trajectory, and τ corresponds to time lag. The MSDs for each bead for a given experimental condition were then averaged.

Extracted values of averaged MSD (including the standard error) were compared at three different time lags (0.2 s, 1 s, and 5 s), which were chosen to represent the data across low, moderate, and high frequencies. MSD magnitudes at the bottom and top layer at specified time lags were compared using Student's t-test.

Particle-tracking microrheology experimental setup for bilayers

To model cardiac tissue in vitro, we deployed a bilayer plating culture using cardiac myocytes and cardiac fibroblasts to engage heterocellular interactions. For these bilayers, cardiac fibroblasts were plated on top of cardiac myocytes (myocytes on top of fibroblasts were unstable). To obtain this bilayer, CMs were first plated on collagen-coated coverslips. After 1 day, the CMs were seeded with 1 μm diameter fluorescent beads and allowed to incubate overnight. On the second day, CFs were plated on top of the CM monolayer, along with additional fluorescent beads. The bilayers were imaged 1 day after plating the CFs. To arrest spontaneous contraction, bilayers were treated with 100 mM KCl in HBSS without calcium and magnesium for 1 h before cell imaging.

For HG experiments, both CMs and CFs were fed low or HG media on the first day after isolation (CFs in separate flask), so that the bilayer was treated for 2 days with the appropriate media. For high-fatty-acid experiments, high-PA or BSA-only medium was added at the time of CF plating. During data acquisition, bead trajectories were acquired for the top layer or bottom layer of cells without explicit identification of the exact cell type. However, our previous work on bilayer plating suggests that CFs on top of CMs are stable in this configuration, whereas if they were swapped, the bilayers tend to lift from the substrate when treated with KCl.

Mirorheological data for bilayers were acquired using HiLo-thresholded analysis as previously reported (25).

Atomic force microscopy

Atomic force microscopy (AFM) was used to compare the stiffness of cardiac myocytes plated on collagen-coated glass coverslips. To arrest spontaneous contraction, myocytes were treated with 100 mM KCl in HBSS without calcium and magnesium for 1 h before cell indentation. An AFM (Bruker, Santa Barbara, CA) mounted on an inverted light microscope (Olympus IX81, Center Valley, PA) was used to measure the elastic moduli of the cells. The cantilever probe used was a silicon-nitride DNP probe (Bruker) with a pyramid-shaped tip and a nominal spring constant of 0.12 N/m. Each cell was indented at 1 Hz in five different locations to find the average Young's modulus for the cell.

The deflection-versus-displacement data were then fit to an 8^{th}-order polynomial (27). The contact point was identified as the first point at which the first and second derivatives were greater than an empirically determined threshold (27). The force was calculated as the product of the cantilever spring constant and the cantilever deflection. We then calculated the point-wise elastic modulus (28) using the equation

$$E = \frac{F(1-\nu^2)}{\pi \times \Phi(D)},$$

where

$$(D) = \frac{4}{3\pi}\left(R^3 D^3\right)^{1/2},$$

when $D<(b^2/R)$ and

$$\Phi(D) = \frac{2}{\pi}\left\{(a\times d) - \left[m \times \left(\frac{a^2}{\tan\phi}\right)\left(\frac{\pi}{2} - \arcsin\left(\frac{b}{a}\right)\right)\right] - \left(\frac{a^3}{3R}\right) + \left(a^2-b^2\right)^{1/2}\left[m\frac{b}{\tan\phi} + \frac{a^2-b^2}{3R}\right]\right\},$$

when $D \geq (b^2/R)$. For this formulation, D is the indentation depth, 2ϕ is the tip angle, b is the radius at which the tapered sides transition into a spherical tip R (set equal to $b = R\cos\phi$), and $m = 2^{1/2}/\pi$ for a pyramid-shaped probe. The contact radius (a) was found by numerically solving the equation

$$D + \frac{a}{R}\left[\left(a^2-b^2\right)^{1/2} - a\right] - \frac{n\times a}{\tan\phi}\left[\frac{\pi}{2} - \arcsin\left(\frac{b}{a}\right)\right] = 0,$$

where $n = 2^{3/2}/\pi$ for a pyramid-shaped probe. Elastic modulus values were statistically compared using Student's t-test.

ROS assay

Intracellular ROS generation was measured with 5(and 6)-chloromethyl-2′,7′-dichlorodihydrofluorescein diacetate, acetyl ester (CM-H2DCFDA). CMs were plated in a 96-well plate. After 2 days, the cells were incubated with HBSS containing 10 μM CM-H2DCFDA at 37°C for 30 min. After 30 min, the cells were washed with warm HBSS three times, and serum-free medium (with various treatments) was added to the wells. The average fluorescence (490 nm excitation, 520 nm emission) for each cell condition was measured with a microplate reader (BioTek, Winooski, VT).

Immunoblotting

Immunoblotting was performed on cells lysed in standard RIPA lysis buffer (Millipore, Billerica, MA) containing 500 nM phenylmethanesulfonyl fluoride, 50 mM sodium fluoride, 1 mM sodium orthovanadate, 10 mM sodium pyrophosphate, and protease inhibitor cocktail (all from Sigma). Samples were solubilized in LDS sample buffer supplemented with 5% w/v 2-mercaptoethanol (Sigma). Total protein concentration was determined by Bradford assay (Sigma). Soluble fractions containing equal amounts of total protein were separated using sodium dodecyl sulfate polyacrylamide gel electrophoresis and transferred onto PVDF membranes (Millipore). Immunoblotting was performed with goat anti-mouse antibodies for cFos (Abcam, Cambridge, MA) (1:250) and TXNIP (MBL International, Woburn, MA) (1:400), followed by horseradish-peroxidase-conjugated goat anti-mouse secondary antibody (Biorad, Hercules, CA) (1:1000). Blots were developed with ECL reagents (Perkin Elmer, Waltham, MA) and imaged using a FUJI imaging unit (Fujifilm, Tokyo, Japan). Relative band intensities in immunoblotting images were quantified using ImageJ, with values normalized to loading control (Beta-tubulin, 1:1000, Sigma).

RESULTS

Diabetic culture conditions stiffen CMs but not CFs

We first assessed whether hyperglycemic and hyperlipidemic conditions associated with diabetes affected the biomechanical properties of cardiac cells. We quantified the rheological properties of CMs using particle-tracking microrheology and found that elevated glucose diminished the MSD of CMs at moderate and high time lags (i.e., moderate and low frequencies (Fig. 1 *A*)). Since diminished MSD is associated with more stiff and/or more viscous properties, these results suggest that diabetic conditions stiffen CMs. Extraction of the complex modulus for the HG indicates that HG-treated myocytes exhibited a larger storage modulus than the control cells over all frequencies, with increased loss modulus at lower frequencies, decreased loss modulus at higher frequencies, and little change at mid-range frequencies. Elevated fatty-acid treatment with PA resulted in significantly diminished MSDs at all examined frequencies (Fig. 1 *B*). The PA-treated CMs exhibited increased storage modulus and loss modulus over all examined frequencies. Either glucose or fatty acids altered passive cell biomechanical properties in a manner consistent with DC. However, fatty-acid treatment exhibited more consistent alterations compared to glucose, which exhibited frequency-dependent effects.

Microrheological results were confirmed using AFM at 1 Hz (Fig. 2, *A* and *B*). Hyperglycemic conditions increase the elastic modulus from 7.49 ± 0.87 to 11.55 ± 1.24 kPa, and hyperlipidemic conditions increase the elastic modulus from 8.68 ± 0.70 to 11.23 ± 1.00 kPa. Further work was done using microrheology alone, since microrheology provides frequency-dependent information for the same cell with a single, passive readout and permits characterization of cell bilayers. Because of the possibility that glucose or fatty-acid treatment would lead to changes in cell mechanics

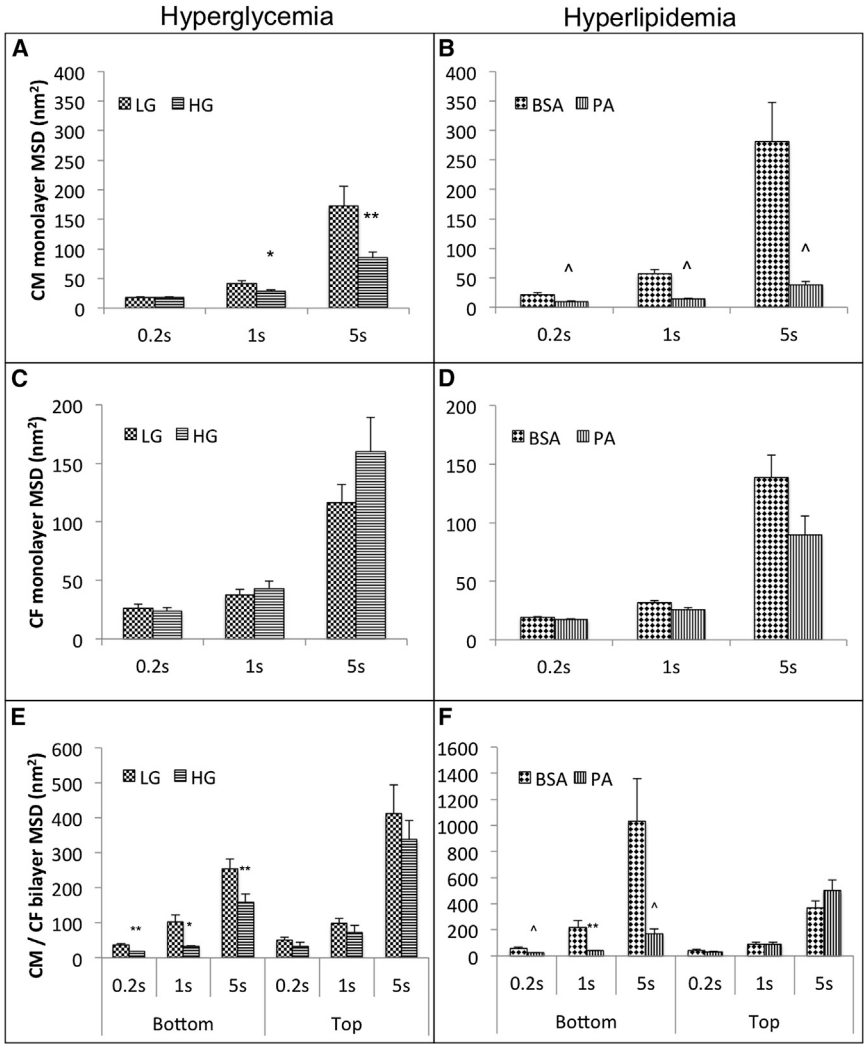

FIGURE 1 Bar plots of MSDs (nm^2) of cardiac myocyte monolayers (*A* and *B*), cardiac fibroblast monolayers (*C* and *D*), and cardiac myocyte/fibroblast bilayers (*E* and *F*) treated with HG (*left column*) or high-fatty-acid conditions (*right column*) at a range of time lags. (*A* and *B*) For monolayers, HG-treated myocytes have a significantly lower MSD at midrange and high time lags (*A*), whereas high-fatty-acid-treated myocytes have a significantly lower MSD over the entire range of time lags (*B*). (*C* and *D*) Neither HG treatment (*C*) nor PA treatment (*D*) has a significant effect on the MSD of CFs compared to control. (*E*) For the glucose-treated bilayer, HG treatment induces a significant increase in MSD at the bottom layer (consisting primarily of CMs) over the entire range of time lags. At the top layer (consisting primarily of CFs), HG treatment produces no significant change in MSD. (*F*) For the PA-treated bilayer, high PA treatment induces a significant increase in MSD at the bottom layer over the entire range of time lags. At the top layer, high PA treatment produces no significant change in MSD. Data are compared using Student's *t*-test ($*p < 0.05$, $**p < 0.01$, $\wedge p < 0.001$).

via significant changes in actin structure or talin localization, we performed actin and talin staining on CMs under control and diabetic conditions. Results indicated no overt differences in actin or talin staining among the four conditions (Fig. 2 *C*).

We next examined CFs and found that their biomechanical properties were mostly invariant to glucose and fatty acid concentration (Fig. 1, *C* and *D*). No significant differences were observed across all examined frequencies.

We then used a coculture condition by plating cardiac fibroblasts atop cardiac myocytes to better mimic cell-cell interactions in vivo. The bottom layer (primarily CMs) exhibited diminished MSD across all examined time lags/frequencies under either elevated glucose or PA treatment, and the top layer (primarily CFs) was not significantly altered (Fig. 1, *E* and *F*). As these results compare relatively well with the results from the monolayer study, we can assume that although some infiltration may have occurred, they did not significantly alter the relative changes in mechanical properties between control and DC conditions. However, with bilayer plating, there were a few notable changes in significance and MSD magnitude. First, the bottom-layer MSD was now significantly different across all time lags, including at 0.2 s, which was not the case in a plain CM monolayer. Second, the control MSD was elevated in the bilayer platings compared to monolayer platings, suggesting that the use of bilayers alters cell biomechanical properties even at baseline. Thus, although cardiac fibroblasts may not directly alter their own characteristics, they likely still regulate CM properties.

ROS treatment does not alter CM stiffness

Elevated ROS is thought to be a key mechanism underlying the progression of DM, and many diabetes studies examine the role of ROS in metabolic pathways. Because both hyperglycemia and hyperlipidemia affected CM properties, we next assessed the potential role of ROS in stiffening these cells. Our results indicated that hydrogen peroxide

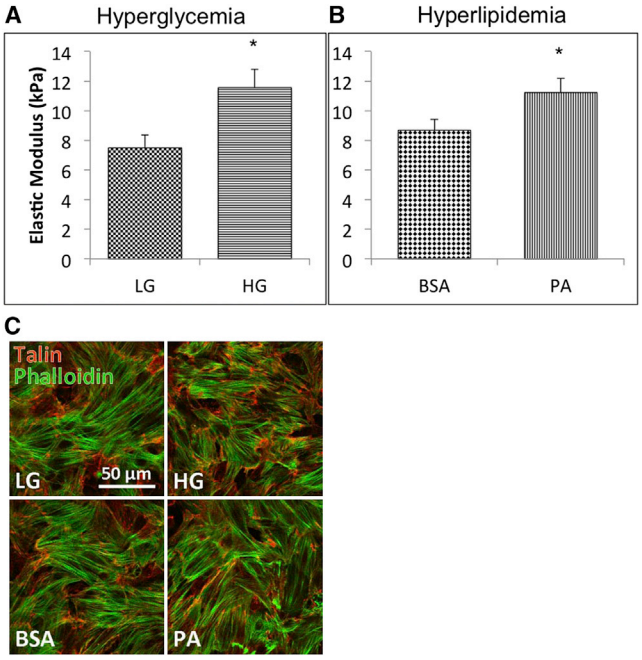

FIGURE 2 (*A* and *B*) AFM measurements on HG-treated cardiac myocytes compared to LG controls (*A*) and on CMs treated with 0.5 mM palmitic acid (PA) compared to BSA-only controls (*B*). Both the HG- and high-PA-treated myocytes experience a significant increase in elastic modulus compared to controls ($p < 0.05$). A double stain using phalloidin to label actin (*green*) and anti-talin antibodies to label talin (*red*) demonstrated no overt differences in stress fiber or talin morphologies or localization under different glucose or fatty acid conditions (*C*). To see this figure in color, go online.

(HP) dosing at 10 μM did not lead to significant changes in cell stiffness, since the MSD (and consequently the G' and G") was not significantly altered under ROS dosing (Fig. 3). Much higher concentrations of HP were avoided due to inimical effects on cells.

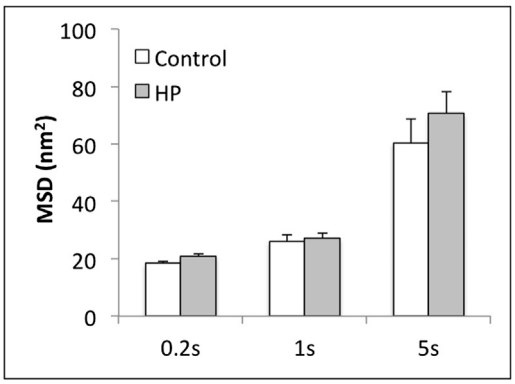

FIGURE 3 Bar plot of the MSD (nm^2) of cardiac myocyte monolayers treated with 10 μM HP compared to treatment with control medium. Hydrogen peroxide treatment does not appear to directly affect the mechanical properties of cardiac myocytes.

Diabetic culture conditions upregulate cFos expression

Another early alteration in DC is the upregulation of hypertrophic pathways. Dosing with HG did not cause a significant change in cFos levels ($p > 0.05$, Fig. 4, *A* and *B*). However, elevated PA exposure significantly increased in cFos, and this increase was reversed by NAC treatment, suggesting that ROS may be involved in cFos regulation in DC ($p < 0.05$; Fig. 4, *C* and *D*). When we dosed with HP, only the highest concentration (50 μM) led to elevated cFos, and cells appeared unhealthy at that dose ($p < 0.05$, Fig. 4, *E* and *F*). Treatment with NAC reversed the HP-induced elevations of cFos (Fig. 4, *G* and *H*). Signaling changes associated with diabetic conditions may be influenced more by fatty acid elevation than by the effects of glucose or ROS alone.

DISCUSSION

We examined the biomechanical, contractile, and hypertrophic properties of cardiac cells exposed to in vitro conditions simulating diabetes. We found that hyperglycemia and hyperlipidemia led to increased stiffness in cardiac myocytes, but not in fibroblasts. These data are consistent with in vivo experiments and epidemiological data, which showed an increase in myocardial stiffness early in the pathogenesis of DC (29,30). Although this increase in myocardial tissue stiffness is likely influenced by increased collagen production of fibroblasts (13), along with the fibrotic replacement of apoptotic/necrotic cells (11), the results presented here suggest that at least some of the increased stiffness in diabetic hearts may be due to an increase in the stiffness of cardiac myocytes themselves at the cellular level. Although the changes in stiffness are not dramatic, they may be enough to cause or contribute to increased cardiac workload over time, leading to DC progression. In contrast, there was no significant change in the mechanical properties of cardiac fibroblasts; however, the presence of fibroblasts in the bilayer plating revealed behavior that was not apparent in the comparably simple monolayers, such as the increased MSD in both cell types when plated together, and the changes to CM properties at low time lags. Thus, in addition to their role in regulating extracellular matrix production, CFs may play an indirect regulatory role in establishing the stiffness of cardiac cells.

Interestingly, treatment with 10 μM HP had no significant effect on CM mechanical properties or cFos levels, suggesting that ROS may have only a limited effect on cardiac cell structural properties. Further, although glucose did affect cell stiffness and contractile dysfunction, it did not alter cFos levels either. Thus, the effects of individual components of glucose, PA, and ROS appear to be multifaceted: different symptoms arise from different, specific, causes. Our findings are consistent with previous literature on

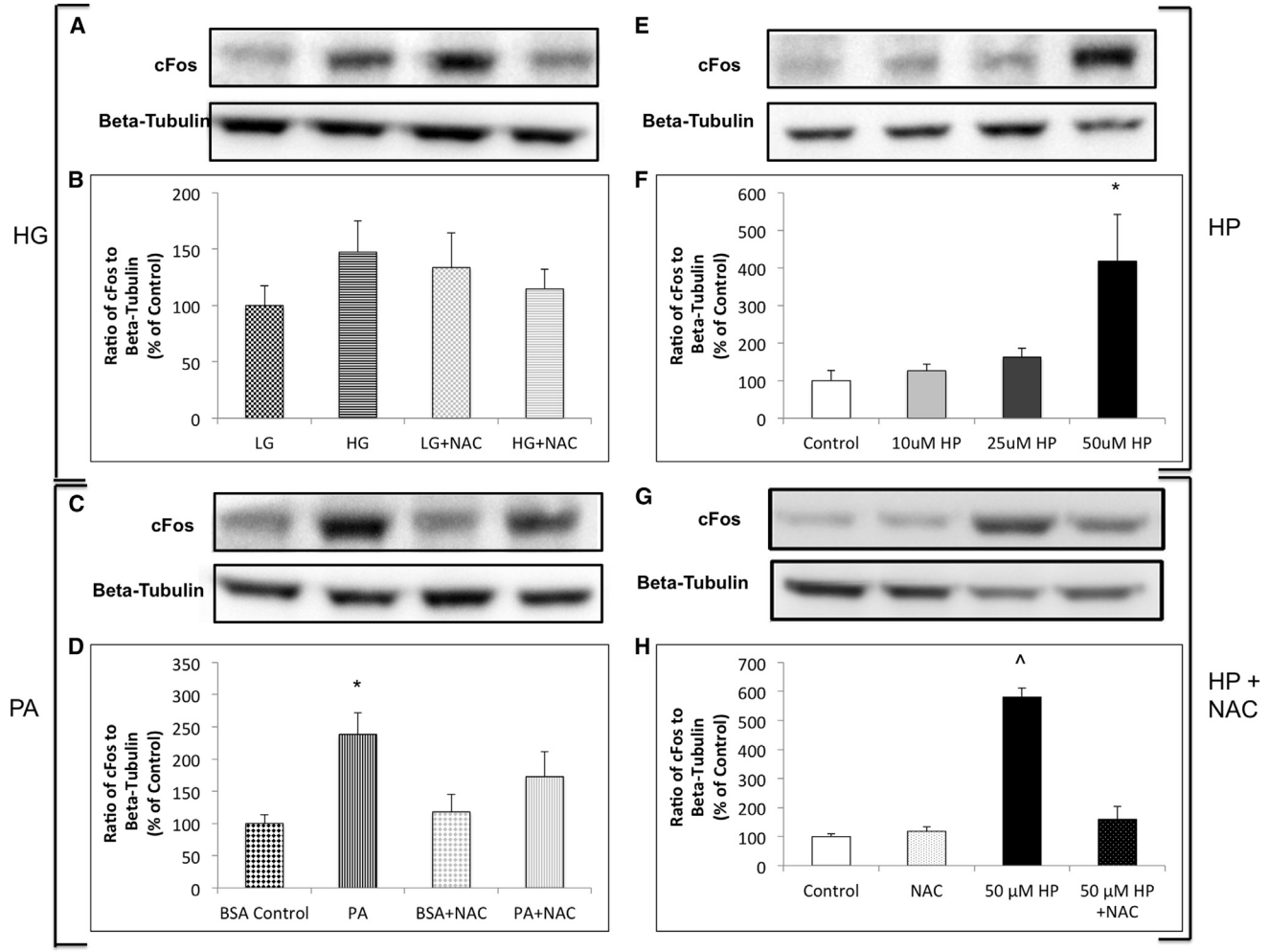

FIGURE 4 (*A* and *B*) cFos levels between LG control and HG-treated CMs with and without NAC had a variable nonsignificant response, with HG-treated CMs experiencing a nonsignificant increase in ROS levels and NAC producing a variable response in both LG control and HG-treated cells. (*C* and *D*) PA-treated CMs see a significant increase in cFos expression, suggesting the presence of hypertrophy in these cells. NAC produces a nonsignificant decrease in cFos expression in PA-treated CMs. (*E* and F).Finally, cFos levels were measured for CMs treated with varying concentrations of HP. cFos levels were found to increase with increasing levels of HP, though these levels were not significantly larger than those measured for controls except in the case of CM treatment with 50 μM HP. (*G* and *H*) Treatment with NAC reduces ROS-induced cFos increase to control levels. The results are shown as the mean $\pm$ SE. Statistical comparisons were made by one-way analysis of variance with a Tukey post-test (*$p < 0.05$; $\wedge$ $p < 0.001$).

DC demonstrating diastolic dysfunction, cFos elevation, and the potentially therapeutic effects of compounds with antioxidant effects on DC (22,31).

To determine whether HG and high fatty acid directly increased cell ROS levels, we measured ROS levels with HG or PA treatment (Fig. S1 in the Supporting Material). The ROS assay did not show a clear change in ROS levels with HG or PA relative to their controls. However, this does not mean that there is no elevation in ROS. The assay was unable to detect ROS up to concentrations that clearly start to affect the viability of cells; at 10 μM, for example, diastolic dysfunction was elevated in CMs. However, the kit was unable to detect such concentrations, and further, NAC treatment suppressed the observed diastolic dysfunction. NAC also suppressed cFos upregulation in PA-treated cells. Thus, it is difficult to assess whether intracellular ROS is altered by glucose or PA treatment and to determine the precise role of ROS in DC. Current research shows a mixed response in ROS production for cardiac cells treated with HG. Although some studies report an increase in ROS levels with 24 h glucose treatment (7,32), other studies either show no significant response (33) or require additional supplements to generate a response (34).

In a similar way, increased expression of the thioredoxin interacting protein (TXNIP) was shown to increase oxidative stress by inhibiting thioredoxin, a protein that modulates the cellular redox state (35,36). Chen et al. found that HG increases TXNIP levels in H9C2 cells, which serve as an immortal analog for cardiac myocytes (37). In addition, NAC has been found to reduce glucose-induced

upregulation of TXNIP in pancreatic β cells (7). However, we found that HG treatment does not have a significant effect on TXNIP levels in CMs, suggesting that this pathway may also have a limited effect in DC (Fig. S2).

The use of microrheology is advantageous in describing the passive properties of cells. However, whether the increase in cell stiffness contributes to overall cardiac stiffening is yet to be determined. In a similar way, spontaneous contractile dysfunction may not be indicative of regulated beating patterns. Interestingly, microrheological responses to PA and elevated glucose exhibited a frequency-dependent effect, with low frequencies (high time lags) typically exhibiting the largest effects. This result suggests that changes to properties (usually stiffening under diabetic conditions) affect the slower characteristics of the cells to a greater extent than the faster responses, such as those during contractions.

In comparing mechanical properties of cells under different conditions, we also attempted microrheological measurements after NAC dosing, but the results were very variable, with cardiac myocytes isolated from different litters yielding different MSDs. This effect may be due to the variability inherent in working with primary cells or to the number of conditions being altered at the same time. It is also possible that NAC has nonlinear effects on cell properties that are not readily modeled using currently available methods. However, we believe that it would be productive to examine the use of antioxidants in modulating the maladaptive alterations in DC-model cell stiffness and hypertrophy in future studies. In a similar way, it may prove fruitful to use combinations of glucose, PA, and ROS, although care must be taken to temper cell stresses. Finally, the differences presented in this article between AFM and microrheology may be due to characteristics of the regions being probed, with AFM yielding cell cortical properties and micorheology yielding internal cytoplasmic properties. Use of other methods to probe biomechanical properties may be helpful. Further establishing and clarifying molecular links and pathways would also likely be useful mechanistic complements to in vivo studies.

Our main conclusions from this study are that 1), diabetic conditions result in changes to cell properties consistent with DC; 2), glucose, PA, and ROS dosing influence different cell properties; and 3), the ROS effect on cells can occur at concentrations that are generally difficult to measure. Thus, the use of bioengineering tools to examine cell properties can offer useful information in understanding DC progression.

SUPPORTING MATERIAL

Two figures are available at http://www.biophysj.org/biophysj/supplemental/S0006-3495(14)00458-5.

This work was supported in part by the National Science Foundation (NSF CBET 1254484).

REFERENCES

1. Hayat, S. A., B. Patel, …, R. A. Malik. 2004. Diabetic cardiomyopathy: mechanisms, diagnosis and treatment. *Clin. Sci.* 107:539–557.
2. Rubler, S., R. M. Sajadi, …, F. D. Holford. 1978. Noninvasive estimation of myocardial performance in patients with diabetes. Effect of alcohol administration. *Diabetes.* 27:127–134.
3. Kiencke, S., R. Handschin, …, P. Rickenbacher. 2010. Pre-clinical diabetic cardiomyopathy: prevalence, screening, and outcome. *Eur. J. Heart Fail.* 12:951–957.
4. Arvan, S., K. Singal, …, A. Vagnucci. 1988. Subclinical left ventricular abnormalities in young diabetics. *Chest.* 93:1031–1034.
5. Galderisi, M., K. M. Anderson, …, D. Levy. 1991. Echocardiographic evidence for the existence of a distinct diabetic cardiomyopathy (the Framingham Heart Study). *Am. J. Cardiol.* 68:85–89.
6. Stone, P. H., J. E. Muller; …, The MILIS Study Group 1989. The effect of diabetes mellitus on prognosis and serial left ventricular function after acute myocardial infarction: contribution of both coronary disease and diastolic left ventricular dysfunction to the adverse prognosis. *J. Am. Coll. Cardiol.* 14:49–57.
7. Xia, Z., K. H. Kuo, …, J. H. McNeill. 2007. N-acetylcysteine attenuates PKCβ2 overexpression and myocardial hypertrophy in streptozotocin-induced diabetic rats. *Cardiovasc. Res.* 73:770–782.
8. Pang, Y., D. L. Hunton, …, R. B. Marchase. 2002. Hyperglycemia inhibits capacitative calcium entry and hypertrophy in neonatal cardiomyocytes. *Diabetes.* 51:3461–3467.
9. Fiordaliso, F., A. Leri, …, J. Kajstura. 2001. Hyperglycemia activates p53 and p53-regulated genes leading to myocyte cell death. *Diabetes.* 50:2363–2375.
10. Anversa, P., and J. Kajstura. 1998. Myocyte cell death in the diseased heart. *Circ. Res.* 82:1231–1233.
11. Kajstura, J., F. Fiordaliso, …, P. Anversa. 2001. IGF-1 overexpression inhibits the development of diabetic cardiomyopathy and angiotensin II-mediated oxidative stress. *Diabetes.* 50:1414–1424.
12. Diogo, C. V., J. M. Suski, …, M. R. Wieckowski. 2013. Cardiac mitochondrial dysfunction during hyperglycemia—the role of oxidative stress and p66Shc signaling. *Int. J. Biochem. Cell Biol.* 45:114–122.
13. Tang, M., W. Zhang, …, Y. Zhang. 2007. High glucose promotes the production of collagen types I and III by cardiac fibroblasts through a pathway dependent on extracellular-signal-regulated kinase 1/2. *Mol. Cell. Biochem.* 301:109–114.
14. Mizushige, K., L. Yao, …, H. Matsuo. 2000. Alteration in left ventricular diastolic filling and accumulation of myocardial collagen at insulin-resistant prediabetic stage of a type II diabetic rat model. *Circulation.* 101:899–907.
15. Stroedter, D., T. Schmidt, …, K. Federlin. 1995. Glucose metabolism and left ventricular dysfunction are normalized by insulin and islet transplantation in mild diabetes in the rat. *Acta Diabetol.* 32: 235–243.
16. Fang, Z. Y., J. B. Prins, and T. H. Marwick. 2004. Diabetic cardiomyopathy: evidence, mechanisms, and therapeutic implications. *Endocr. Rev.* 25:543–567.
17. van Heerebeek, L., N. Hamdani, …, W. J. Paulus. 2008. Diastolic stiffness of the failing diabetic heart: importance of fibrosis, advanced glycation end products, and myocyte resting tension. *Circulation.* 117:43–51.
18. Turan, B. 2010. Role of antioxidants in redox regulation of diabetic cardiovascular complications. *Curr. Pharm. Biotechnol.* 11:819–836.
19. Seddon, M., Y. H. Looi, and A. M. Shah. 2007. Oxidative stress and redox signalling in cardiac hypertrophy and heart failure. *Heart.* 93:903–907.
20. Liu, Y., S. Lei, …, Z. Xia. 2012. PKCβ inhibition with ruboxistaurin reduces oxidative stress and attenuates left ventricular hypertrophy and dysfunction in rats with streptozotocin-induced diabetes. *Clin. Sci.* 122:161–173.

21. Santalucía, T., M. Christmann, …, N. J. Brand. 2003. Hypertrophic agonists induce the binding of c-Fos to an AP-1 site in cardiac myocytes: implications for the expression of GLUT1. *Cardiovasc. Res.* 59:639–648.

22. Min, W., Z. W. Bin, …, F. G. Sheng. 2009. The signal transduction pathway of PKC/NF-κ B/c-fos may be involved in the influence of high glucose on the cardiomyocytes of neonatal rats. *Cardiovasc. Diabetol.* 8:8.

23. Leroy, C., S. Tricot, …, A. Grynberg. 2008. Protective effect of eicosapentaenoic acid on palmitate-induced apoptosis in neonatal cardiomyocytes. *Biochim. Biophys. Acta.* 1781:685–693.

24. Jonas, M., H. Huang, …, P. T. So. 2008. Fast fluorescence laser tracking microrheometry, I: Instrument development. *Biophys. J.* 94:1459–1469.

25. Michaelson, J., H. Choi, …, H. Huang. 2012. Depth-resolved cellular microrheology using HiLo microscopy. *Biomed. Opt. Express.* 3:1241–1255.

26. Shen, M. Y., J. Michaelson, and H. Huang. 2013. Rheological responses of cardiac fibroblasts to mechanical stretch. *Biochem. Biophys. Res. Commun.* 430:1028–1033.

27. Elkin, B. S., E. U. Azeloglu, …, B. Morrison, 3rd. 2007. Mechanical heterogeneity of the rat hippocampus measured by atomic force microscope indentation. *J. Neurotrauma.* 24:812–822.

28. Lin, D. C., E. K. Dimitriadis, and F. Horkay. 2007. Robust strategies for automated AFM force curve analysis—I. Non-adhesive indentation of soft, inhomogeneous materials. *J. Biomech. Eng.* 129:430–440.

29. Falcão-Pires, I., and A. F. Leite-Moreira. 2012. Diabetic cardiomyopathy: understanding the molecular and cellular basis to progress in diagnosis and treatment. *Heart Fail. Rev.* 17:325–344.

30. Loganathan, R., M. Bilgen, …, I. V. Smirnova. 2006. Characterization of alterations in diabetic myocardial tissue using high resolution MRI. *Int. J. Cardiovasc. Imaging.* 22:81–90.

31. Ramírez, E., M. Klett-Mingo, …, O. Lorenzo. 2013. Eplerenone attenuated cardiac steatosis, apoptosis and diastolic dysfunction in experimental type-II diabetes. *Cardiovasc. Diabetol.* 12:172.

32. Yu, T., J. L. Robotham, and Y. Yoon. 2006. Increased production of reactive oxygen species in hyperglycemic conditions requires dynamic change of mitochondrial morphology. *Proc. Natl. Acad. Sci. USA.* 103:2653–2658.

33. He, X., H. Kan, …, Q. Ma. 2009. Nrf2 is critical in defense against high glucose-induced oxidative damage in cardiomyocytes. *J. Mol. Cell. Cardiol.* 46:47–58.

34. Kumar, S., and S. L. Sitasawad. 2009. N-acetylcysteine prevents glucose/glucose oxidase-induced oxidative stress, mitochondrial damage and apoptosis in H9c2 cells. *Life Sci.* 84:328–336.

35. Junn, E., S. H. Han, …, I. Choi. 2000. Vitamin D3 up-regulated protein 1 mediates oxidative stress via suppressing the thioredoxin function. *J. Immunol.* 164:6287–6295.

36. Nishiyama, A., H. Masutani, …, J. Yodoi. 2001. Redox regulation by thioredoxin and thioredoxin-binding proteins. *IUBMB Life.* 52: 29–33.

37. Chen, J., H. Cha-Molstad, …, A. Shalev. 2009. Diabetes induces and calcium channel blockers prevent cardiac expression of proapoptotic thioredoxin-interacting protein. *Am. J. Physiol. Endocrinol. Metab.* 296:E1133–E1139.